Chemical Engineering Science 196 (2019) 527–537

Contents lists available at ScienceDirect

Chemical Engineering Science

journal homepage: www.elsevier.com/locate/ces

Characterization of products derived from the high temperature flash pyrolysis of microalgae and rice hulls

Aaron W. Palumbo, Christopher J. Bartel, Jeni C. Sorli, Alan W. Weimer *

Department of Chemical and Biological Engineering, University of Colorado at Boulder, Boulder, CO 80303, United States

HIGHLIGHTS

- Microalgae and rice hulls were flash pyrolyzed in a drop-tube reactor at 1300–1600 °C.
- Syngas and biochar were formed; condensable products were negligible.
- Chars became similar in physio-chemical properties, independent of starting material.
- A conceptual solarthermal operating configuration was introduced.

ARTICLE INFO

Article history:
Received 2 September 2018
Received in revised form 8 November 2018
Accepted 11 November 2018
Available online 12 November 2018

Keywords:
Biochar
Flash pyrolysis
Syngas
Drop-tube

ABSTRACT

Flash heating and high temperature processing of two biomass feed materials is presented as a sustainable thermochemical technique to leverage the entire carbon content of the starting material for various end-uses. Microalgae and rice hulls were flash pyrolyzed in a drop-tube reactor to form exclusively gas and solid products in the temperature range 1573–1873 K at gas residence times of 3–5 s. Product gas yields and compositions approached thermodynamic equilibrium predictions with increasing temperature, which were used in calculations for a conceptual solarthermal processing framework. The derived carbonaceous residue was further characterized for composition (atomic mass and crystalline structures), morphology (surface area, pore volume, surface roughness), and reactivity (*via* CO_2 thermogravimetry). Solid residues generated under flash conditions tended to become nearly indistinguishable, becoming spherical with high macroporosities and similar apparent reactivities. These results were contrasted with slow-pyrolyzed chars of the same starting materials, whose characteristics were markedly opposite for microalgae and rice hulls, further evidencing the importance of char particle thermal history. Results from solarthermal operation show a high calorific value syngas, especially for microalgae at 1873 K. The applicability of carbonaceous residue in a particular downstream use requires further characterization and study.

1. Introduction

Thermochemical conversion of biomass includes a complex set of processing technologies suited to address sustainable production of fuels, chemicals, and power. Pyrolysis represents one major classification of thermochemical techniques, and is broadly defined as the thermal decomposition of a bio-based feed material forming primarily permanent gases, condensable vapors, and a carbonaceous solid residue. However, the processing technique of biomass pyrolysis belies the strict scientific notion of the term. In fact, the high-level category of pyrolysis as a process involves chemical phenomena that are not always pyrolytic, *and* whose performance is intimately affected by physical phenomena such as heat transfer to and through a particle (Babu, 2008; Di Blasi, 2008). Indeed, pyrolysis is generally sub-classified primarily by particle heating rate regimes of slow, fast, and flash with no standardized boundaries and with no regard to desired products (Vamvuka, 2011). One could argue that the pyrolysis of biomass is a misnomer altogether since biomass is generally highly oxygenated and oxidizes itself during any high temperature process, becoming very similar to the process of gasification and severely limiting the total yield of hydrocarbons that could be formed as an end-product (Tanger, 2013; Singh, 2010). The distinguishing features of pyrolysis technologies and the language used to describe them, then, still need further resolution and precision. The identity of pyrolysis processing is further exacerbated by operating configurations that do not dwell within the standard connotations of desired outcomes,

* Corresponding author.
E-mail address: alan.weimer@colorado.edu (A.W. Weimer).

https://doi.org/10.1016/j.ces.2018.11.029
0009-2509/

namely, when char or gas products are desired over condensable liquids such as in flash pyrolysis reactors. In many conventional cases, char and permanent gases are byproducts that must be 'dealt with.' For char at least, agricultural applications (e.g. soil amendment) have emerged as one of the more promising disposal routes. Yet many considerations have been given to the indirect pyrolyzer where char is combusted, despite the relatively high cost of delivered and dried biomass per unit of energy.

It is of utmost importance for engineers studying thermochemical conversion technologies to classify their processes with respect to products formed and the conditions of their reactor system (Agrawal and Sikdar, 2012; Qureshi, 2018). Generally, 'pyrolysis' is used to denote the directed formation of liquid products, gasification for gaseous products, and carbonization for solid products. In reality, all three product variations are usually formed and retained at the exit of the reactor system. However, ignoring the non-negligible quantities of undesired products in order to extrapolate a higher level categorization of a given technology can lead to oversight of unit operations needed to produce a marketable end-product (Brown and Stevens (2011)).

The flash pyrolysis of biomass, for instance, has been studied at moderate temperatures, focusing on optimization of the condensable liquid portion of products, as is the common approach for pyrolysis processing (Di Blasi et al., 2000; Dufour, 2011; Dupont, 2009; Janse et al., 2000; Scott and Piskorz, 1982). However, flash pyrolysis has been shown to be highly limited by heat and mass transport phenomena, indicating high difficulty in controlling the reaction processes to optimize one fraction over another (Dufour, 2011; Palumbo and Weimer, 2015). Similarly, flash pyrolysis is often grouped with ablative pyrolysis, where substantial internal pressure causes particle rupturing and size reduction and therefore decreased heat transfer resistance (Vamvuka, 2011). However, biomass particles exposed to extreme radiation sources do not always ablate, especially since heat transfer is extremely limiting to the surface of the particle and for particles with very low thermal diffusivities, as most have.

As such, flash pyrolysis of biomass has not received significant attention in the literature, partially due to the connotation that pyrolysis is associated with liquid products, which are obtained in higher yields using other pyrolysis technologies (Vamvuka, 2011; Garcia-Nunez, 2017; Aarum, 2017; Maliutina, 2017). Yet, flash pyrolysis represents a simpler operating paradigm that can be used to avoid many of the tireless pitfalls that have befallen commercial application of pyrolysis technologies (e.g. fouling, low yields, use of undesired fraction). In fact, high temperature flash pyrolysis is akin to gasification in that the permanent gas fraction and char products are both desired fractions. Indeed, it is known that sufficiently high temperatures and residence times can lead to complete thermal destruction of tar compounds, a mark of categorizing such a process under the banner pyrolysis as opposed to gasification (Dufour, 2011; Milne, 1998; Qin, 2012, 2013; Devi et al., 2003). Though it is believed that either name could be used underlining the importance of creating high-level conceptual artwork in ways that are inclusive to the entire range of possible operating scenarios (Arregi, 2018).

Biochar as a primary desired product can function as a secondary fuel source to derive heat and power, or utilized for non-fuel applications such as a soil amendment for crops or water treatment absorbent (Cha, 2016; Lee, 2010; Manya, 2012). The problem of thermochemical processes with focus on fuel production implies that the char product will not be engineered to accommodate many of these emergent end-uses (Sun, 2012). Nevertheless, char activation and preparation has become a large topic of study, remaining fairly agnostic to the methods used to derive the chars (Cha, 2016). Understanding how the conditions of generating chars lead to specific characteristics can lead to engineered chars within thermochemical processes that do not necessarily consider char as the primary desired product (Asadullah, 2010; Biagini et al., 2008; Brewer, 2009; Cetin, 2004).

Presented is a high temperature thermochemical process to produce synthesis gas and char products exclusively, avoiding condensable tars. This operating regime has received little attention in the literature and often does not fall into any of the broad classifications formulated by some purveyors. Two compositionally dissimilar biomass feed materials (microalgae and rice hulls) were initially dried, ground, and sieved then sent through a high temperature drop-tube reactor at temperatures between 1573 and 1873 K. Condensable liquids were not observed resulting in the primary formation of carbonaceous residue and synthesis gas (syngas). The syngas products were analyzed for composition and heating value whereas the carbonaceous residue was characterized with respect to composition, morphology, and reactivity as a starting point for comprehensive life-cycle analysis in a given end-use. The chars derived under flash heating conditions were compared to those generated in a slow heating regime to demonstrate the range of possible char characteristics. Using experimental results, the authors also present a process synthesis for a solarthermal system to address industrial sustainable production of synthesis gas and char products complete with a characteristic time analysis as an overview presentation of reactor design challenges.

2. Materials and methods

2.1. Materials

Two raw biomass sources were used, microalgae and rice hulls, representing vastly different biochemical (not shown) and atomic compositional profiles. Spray-dried microalgae (*Chlorella*) were obtained from Arizona Public Services. Ground rice hulls were obtained from Sundrop Fuels, Inc. (Longmont, CO). Both raw materials were sieved (100–200 mesh [75–150 μm sieve diameter]) prior to analysis and pyrolysis experiments. Table 1 displays the ultimate and proximate compositions of each raw material. These analyses were performed by Huffman Laboratories (Golden, CO) using LECO combustion analysis for atomic compositions (ASTM E777, E778, E775), oven drying for moisture content (ASTM E871), and bomb calorimetry for higher heating value (ASTM D5865). The sieve fraction used in experiments was also used in compositional analysis.

2.2. Experimental

Both raw biomass samples were dried prior to pyrolysis experiments. However, due to uncontrollable reabsorption of atmospheric

Table 1
Proximate and ultimate analyses of microalgae and rice hulls used in pyrolysis experiments.

dry wt%	Microalgae	Rice Hulls
C	51.7	39.4
H	7.19	5.23
O (diff)	28.9	34.7
N	8.81	1.03
S	0.48	0.10
Ash	2.93	19.5
Dry ash free basis [mol/mol]		
O/C	0.420	0.663
H/C	1.658	1.583
N/C	0.146	0.022
S/C	0.004	0.001
As received basis		
Moisture [wt%]	4.50	4.50
HHV [MJ/kg]	23.07	15.16

humidity during experimental set-up, the actual moisture content was between 2 and 5 wt%, as measured by a second round of drying after allowing the biomass to equilibrate with the atmosphere for several hours. Pyrolysis was conducted in two separate configurations to facilitate 'slow' and 'flash' conditions, corresponding to particle heating rate. Slow pyrolysis was performed exclusively as a point of comparison for biochar characteristics, not for process performance. Since there are no standardized definitions for these terms, slow pyrolysis denotes a reactor heating rate of 5 K/min. The authors acknowledge that the reactor heating rate is an upper limit to the actual heating rate of the sample (Lede, 2010). Flash pyrolysis denotes rapid radiative heating to the particle surface at calculated heating rates greater than 1000 °C/s. The conditions facilitating flash conditions, as opposed to fast heating, was previously outlined in Bahng (2009).

Slow pyrolysis was conducted in an electric horizontal tube furnace (Carbolite STF) using a 50 mm OD alumina tube. The sieved biomass sample (10–15 g) was placed uniformly in a quartz boat in the middle of the reactor. Nitrogen gas was initially set at 2 slpm to purge the system of oxygen (<100 ppm), then fixed at 0.5 slpm for experiments. The furnace heating rate was set to 5 K/min, reaching a maximum setpoint temperature of 1073 K. The sample was held at 1073 K for 30 min, then the reactor was set to cool at a rate of 5 K/min. Analysis of product gases and condensables was not performed. However, the product gas stream was sent through a 1.0 M NaOH solution at 273 K to remove and neutralize condensable vapors and soot. Permanent gases were vented. After the furnace was cooled, the solid char residue was collected for analysis and stored in a vacuum desiccator.

Flash pyrolysis was performed in a 60 kVA electric vertical tube furnace (Thermal Technologies Astro series) using a 0.1 m OD alumina tube (Fig. 1). The tube was heated externally by a graphite heating element with a uniform hot zone length of 0.45 m. Reactor temperatures were measured at the external tube wall and set to 1573–1873 K. Temperatures were measured using a type C thermocouple and a dual wavelength IRCON pyrometer. These temperatures are not necessarily the operating temperature of the reacting medium, nor was it determined whether the reactants reach these set-point temperatures. Once the setpoint temperature was reached the system was allowed to equilibrate for 1 h. Biomass was then fed into the reactor at feed rates between 5 and 20 mg/s using a pneumatic brush feeder facilitated by 1.0 slpm of N_2 sweep gas (Woodruff et al., 2012). Additional diluent sweep gas was heated to 500 °C and entered the reactor through a side port and was used to control gas residence time on the order to 3–5 s. The reactor configuration is a drop-tube, implying non-aerosol particles. However, the residence time of the solids was unknown because of likely natural convection currents within the reactor, an unmeasured buoyancy of solids, and dramatic changes in size, shape, and density of the solids during the pyrolysis process. Nevertheless, the minimum residence time of the solids was calculated at 0.1 s assuming standard falling object physics.

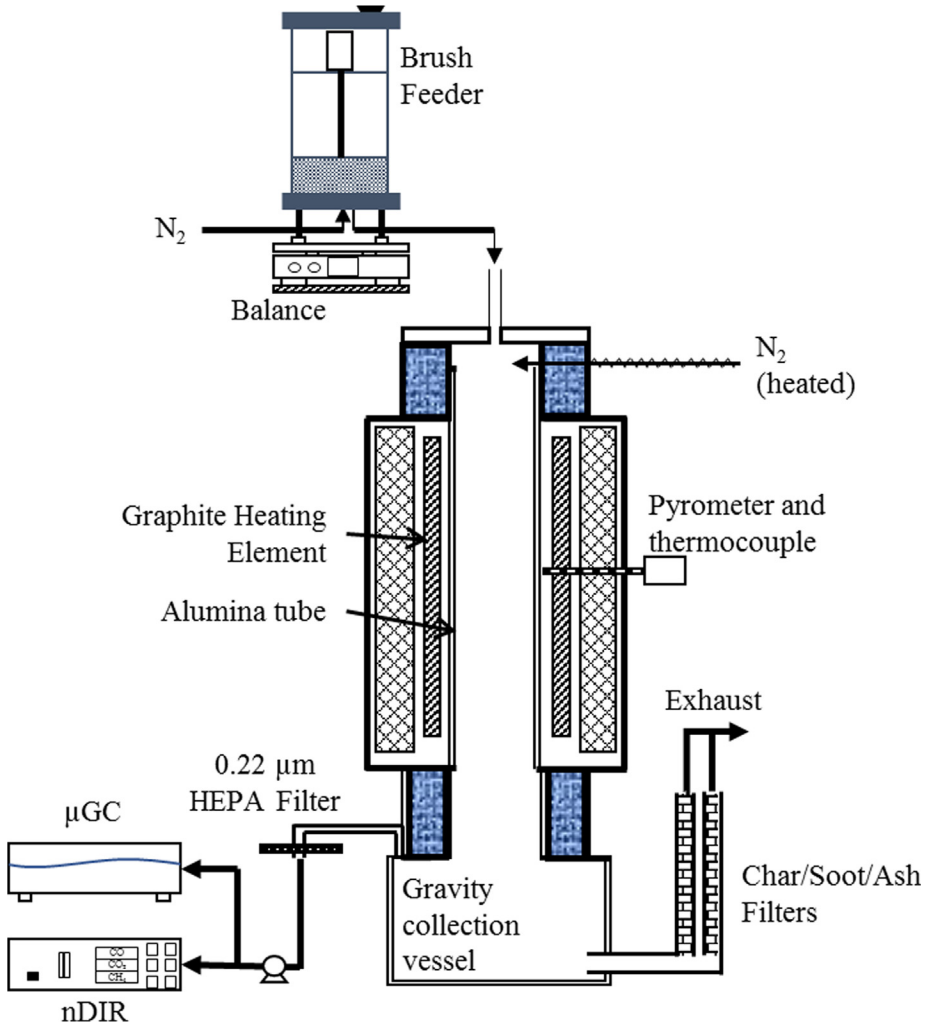

Fig. 1. Schematic of the high temperature flash pyrolysis system.

Products were immediately cooled by flowing through a water-cooled region at the bottom of reactor tube. Residual char and soot was collected in a gravity vessel, on fiberglass mesh filters, and stainless steel canister filters. It was found that char primarily collected in the gravity vessel and fiberglass mesh whereas soot collected primarily on the stainless steel canister filters. Tar formation was not observed anywhere in the collection zone. Product gases were sent through an online continuous non-dispersive infrared detector (California Analytical Instruments ZRE nDIR) for CO, CO_2, and CH_4. H_2 and N_2 were measured using a Varian CP-4900 μCG with Mol Sieve 5A and Poruplot X columns at a sample time of 60 s. It was assumed that the total moles of nitrogen in the product gas were equal to the total moles of gas sent into the system plus the nitrogen content of the biomass sample (determined to be negligible). From previous experiments, it was known that the presence of C_{2+} hydrocarbons would be negligible (Palumbo and Weimer, 2015; Palumbo et al., 2015). After each experiment, the solid product was collected and stored in a vacuum desiccator. The system was left hot during this period and had to be purged of oxygen prior to subsequent runs.

2.3. Analysis of solid residue

The solid carbonaceous residue was characterized quantitatively for atomic composition, surface area, size, pore volume, apparent reactivity, and qualitatively for macroporosity (surface roughness) and degree of graphitization.

Atomic composition was determined using the same methods described above for the raw biomass samples. Char surface area was determined using BET isotherm analysis (Micromeritics ASAP 2010, 77 K under N_2), resulting primarily in type 2 or 3 IUPAC adsorption isotherms for flash-pyrolyzed samples, indicating a high macroporosity. Concurrent with surface area analysis, pore volume was determined using BJH desorption isotherm analysis. Both BET and BJH sample preparation entailed vacuum drying samples overnight at 105 °C. Relative pressures ranged from 10^{-4} to 0.99.

Particle sizes were indicated using equivalent spherical diameter and aspect ratio. Scanning electron micrographs (SEM) were obtained with approximately 100–200 particles. At least 500 particles were imaged and analyzed for size using the software ImageJ. SEM's were prepared using gold sputtering to improve conductivity of samples and prevent sample charging.

SEM's were also used for qualitative examination of macroporosity and surface roughness. Surface roughness was correlated to pixel intensity of at least five micrographs, each containing 100–200 particles. Greyscale assignments were based on 0 (white) to 256 (black) as described by the method reported by Biagini et al., and Matlab was used for pixel analysis of the micrographs (Biagini et al., 2008).

X-ray diffraction (XRD) was used to explore the degree of graphitization of char samples using a similar methodology to Cetin et al. (2005). This analysis was also qualitative in nature, with visual inspection of the peaks at $2\Theta \approx 25, 42$ where crystalline carbon (graphite) is identifiable.

Thermogravimetric analysis (TGA) was performed on slow and flash pyrolyzed chars to determine apparent reactivity in CO_2 atmospheres at 1273 K. TGA runs were performed in duplicate in a Netsch STA 449 F1 Jupiter thermogravimeter with alumina crucible and set at a heating rate of 10 K/min and hold time of 120 min. Sample reactivity was calculated using a basic mass loss rate expression dm(t)/dt and normalized to the total quantity of mass lost for each experiment to obtain a dimensionless conversion rate R(t) = dx/dt where conversion is a continuous function from 0 to 1.

3. Results and discussion

3.1. Characterization of solid residue

The solid fraction derived from the pyrolysis of biomass is generally classified as char. However, in the experimental system used where high temperatures of the particle *and* fluid phases are obtained, the volatile organic components that evolve from a given particle continue to react and agglomerate to form soot and more permanent gases via secondary pyrolysis pathways. Likewise, the ash portion can often undergo compositional changes, though it is commonly held that most of the inorganic portion remains within the solid residue with small amounts of chlorine- and nitrogen-containing compounds having formed into permanent gases. Constituents that originally volatilize during the reaction, such as high molecular weight aromatics, alkali and alkaline metals, sulfur compounds, and others, condensed or deposited with the solid carbonaceous residue or at other points downstream. Therefore, the collected products from high temperature flash pyrolysis are either permanent gases and carbonaceous solid, the latter including all solid deposits collected. Separation of the varieties of solid products (soot, ash, char) was not attempted.

3.1.1. Compositional analysis

An ultimate analysis of a bulk solid residue is shown in Table 2 with char derived from slow pyrolysis as a point of comparison. In general, the microalgae char retained a large amount of mass within the solid residue, about 42% and 34% for slow and flash pyrolysis (d.a.f. mass basis), respectively. This may be a direct outcome of the starting composition in terms of oxygen and hydrogen whose desire to leave the particle associated with carbon as a hydrocarbon is well known. For rice hulls, the volatile content was much larger where the remaining char fraction was only 28% and 18% for slow and flash pyrolysis (d.a.f. basis), respectively. The correlation of initial oxygen and hydrogen content was apparent as rice hulls are lignocellulosic with significantly more oxygen.

Overall, in comparison with Table 1, hydrogen and oxygen were shown to favor the gas fraction of products leaving behind a solid carbon matrix infused with a large inorganic portion. The severity of pyrolysis temperature shows a correlation with a loss of hydrogen and oxygen. Slow pyrolysis rates resulted in a less severe decrease of these constituents indicating that heating rate is an important measure of total evolved volatile content. The differences between slow and flash pyrolyzed biomass is most notable from the remaining nitrogen and sulfur content. Slow pyrolysis does not seem to drive away nitrogen but almost completely eliminates all sulfur. The opposite is true of flash pyrolyzed biomass, nitrogen evolves readily but sulfur remains. Therefore, it is likely that sulfur initially volatilizes during pyrolysis. However, it is unclear is sulfur-containing gases decompose at high operating temperatures, facilitating the deposit of sulfur in the collected solids, or if sulfur and its volatile compounds would remain in the permanent gas stream at less severe conditions. Interpreting the results from slow pyrolysis, it appears that nitrogen remains within the particle at slow heating rates but is evolved at flash heating rates, most likely in the form of N_2 as predicted by thermodynamic equilibrium.

X-ray diffraction spectra (Fig. 2) qualitatively revealed increased carbon graphitization in microalgae char with increasing heating rate. This was not the case for rice hull char which remained amorphous even at a furnace temperature of 1873 K. Fig. 2 summarizes the results from XRD. Fig. 2(b) shows a sharp peak increasing in size with increasing heating rate at a 2θ angle of about 28° which represents crystalline silica and is more pronounced at high heating rate due to the increased ash content of

Table 2
Ultimate analyses for carbonaceous products generated under slow and flash heating conditions for microalgae and rice hulls.

Temperature	Microalgae ($C_1H_{1.66}O_{0.42}$)										
	Equilibrium [mol/mol$_{bio,daf}$], [kJ/mol$_{bio,daf}$]						Experiment [mol/mol$_{bio,daf}$], [kJ/mol$_{bio,daf}$]				
	H_2	CO	CO_2	CH_4	$C_{(s)}$	LHV	H_2	CO	CO_2	CH_4	LHV
1573 K	0.63	0.32	0	0	0.58	242	0.29	0.20	0.01	0.01	135
1673 K	0.63	0.32	0	0	0.58	242	0.34	0.26	0.00	0.00	158
1773 K	0.63	0.32	0	0	0.58	242	0.31	0.34	0	0	171
1873 K	0.63	0.32	0	0	0.58	242	0.44	0.33	0	0	198
Temperature	Rice Hulls ($C_1H_{1.58}O_{0.66}$)										
	Equilibium [mol/mol$_{bio,daf}$], [kJ/mol$_{bio,daf}$]						Experiment [mol/mol$_{bio,daf}$], [kJ/mol$_{bio,daf}$]				
	H_2	CO	CO_2	CH_4	$C_{(s)}$	LHV	H_2	CO	CO_2	CH_4	LHV
1573 K	0.54	0.45	0	0	0.34	257	0.39	0.40	0.02	0.01	217
1873 K	0.54	0.45	0	0	0.34	257	0.56	0.43	0	0	257

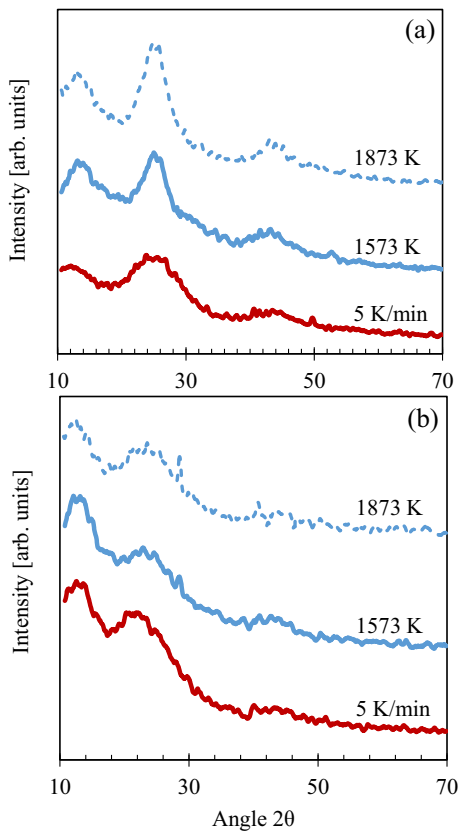

Fig. 2. X-ray diffraction spectra for chars of (a) microalgae and (b) rice hulls derived under slow and flash heating conditions.

the chars and high temperatures involved to crystallize silica in rice hulls, which are known to have high silica content relative to other biomass (Tanger, 2013). The sharpening of the peak at $2\theta = 25°$ in Fig. 2(b) is indicative of the [0 1 0] crystal plane of graphitic carbon. There is also slight suggestion of an increase at $2\theta = 42°$ representing the [2 0 0] crystal plane. Graphitic carbon is known to be less reactive than amorphous carbon due to its relative stability compared to other carbon types (Sun, 2012; Cao, 2012). This could have a significant impact on carbon recalcitrance for soil applications.

3.1.2. Morphology

Scanning electron micrographs (SEM's) revealed that microalgae were initially near-perfect spheres in contrast to the ground rice hulls which formed fibrous cylinders. Fig. 3 displays a sample of the parent biomasses as well as chars derived under slow and flash pyrolysis conditions. Fig. 4 contains population distribution results from SEMs analyzed in the software package ImageJ for equivalent spherical diameter and aspect ratio. Population distributions for flash pyrolyzed biomass at different temperatures were all indistinguishable, therefore only results from 1873 K are displayed. From both these Figures, it is apparent that flash pyrolysis results in smaller particles with a highly spherical shape, or low aspect ratio. Because microalgae begin as near-perfect spheres, Fig. 4(a) shows a slight increase in aspect ratio. Rice hulls reveal a dramatic decrease in aspect ratio. In combination with a much smaller particle size, the rice hulls were thought to have fragmented into smaller pieces due to the large flux of gases and overpressure resulting from flash pyrolysis. This was not seen during slow pyrolysis where rice hulls maintained both size and shape, indicating that flash heating rates causes severe structural reorganization of the underlying carbon-ash matrix. It has previously been shown that biomass can form a meta-stable molten phase during rapid heating conditions, which would lead to creating spherical globules. Additionally, rice hull ash is composed predominately of silica, which has a relatively low melting point and may contribute to the overall globule-shaped char particles as a direct consequence of this softening or melting causing droplet formation. For both biomasses, the general shape of the parent material is preserved due to slow evolution of gases implying minimal physical re-structuring during char formation as well as a low degree of interaction between flowing gases and the particle.

SEM's were also used to qualitatively explore surface macroporosity, or surface roughness, by analyzing pixel intensity in Matlab. Biagini et al reported a correlation between porosity and pixel population distribution (Biagini et al., 2008). In their results, the parent biomass material was characterized by low porosity and surface area, leading to a relatively smooth surface compared to the char product whose surface was marred with craters and holes created by the loss of mass and flow of volatiles through the particle. In Fig. 5, the results from the pixel analysis are displayed. The curves of pyrolyzed biomass do not reveal a broadening of the distribution. For microalgae, the slow pyrolyzed char is essentially overlaid onto the results for the raw material. This is not surprising since Fig. 3 revealed almost identical general appearance. The flash pyrolyzed microalgae have an increased peak height and a slight shift toward black which may be indicative of an increased in the quantity of holes. For rice hulls, slow pyrolyzed char resulted in a narrower curve with increased peak height and shift toward white. Flash pyrolyzed rice hulls showed intermediate results between the slow pyrolyzed and raw material. These results imply that flash pyrolyzed chars become smooth with relatively low macroporosity compared to the slow pyrolyzed char, the opposite of that which occurred for microalgae.

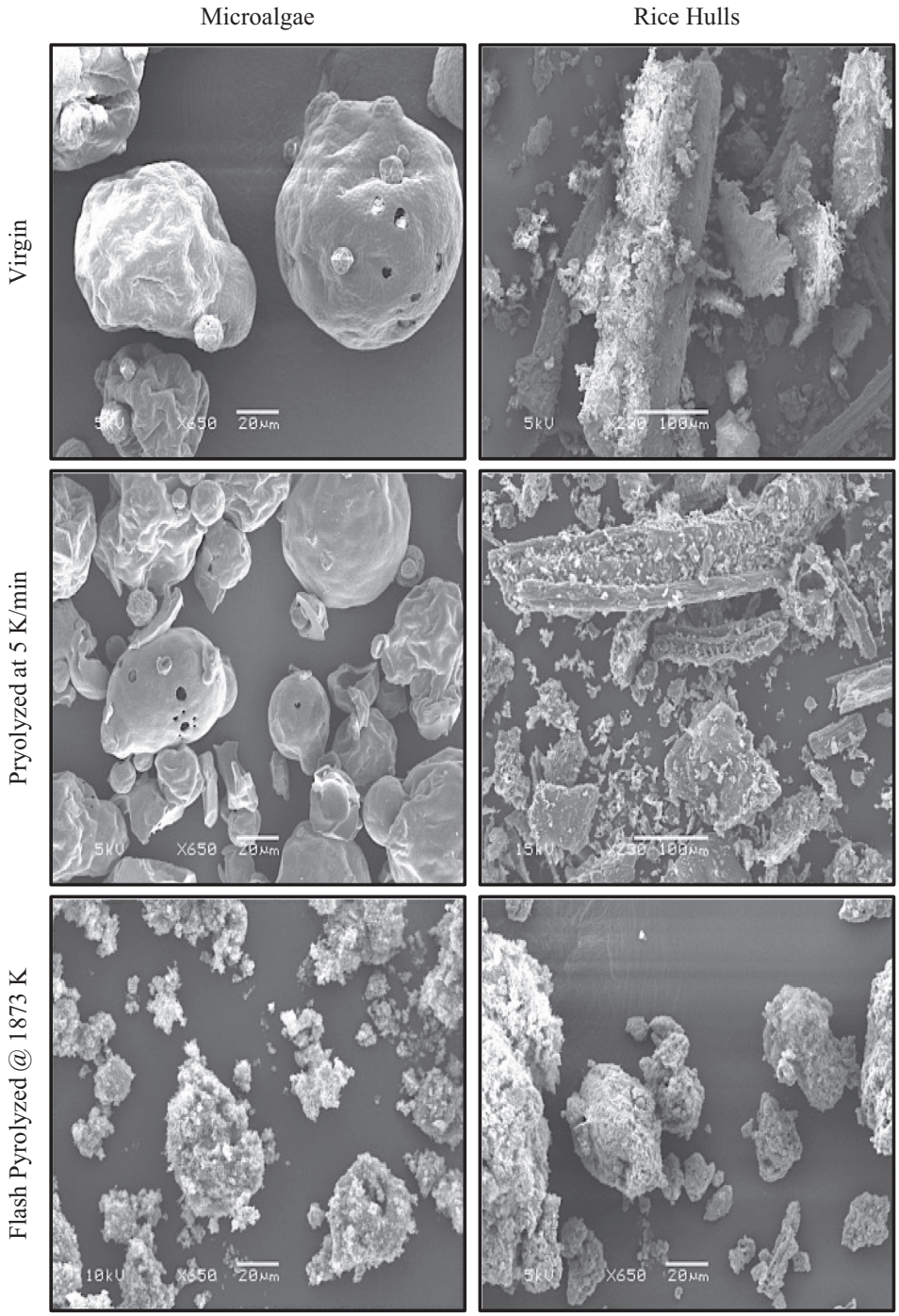

Fig. 3. Scanning electron micrographs of microalgae, rice hulls, and their respective chars derived under slow and flash heating conditions.

3.1.3. Pore area and volume

Results from BET surface area analysis and BJH desorption are shown in Table 3. The pore diameter range was from 2 to 250 nm and is correlated to cumulative pore volume and area. Both microalgae and rice hulls contained similar results except in the case of slow pyrolyzed chars. Slow pyrolyzed microalgae char underwent a reduction in surface area and pore volume/area. In addition to the shrinkage, the resulting slow pyrolyzed microalgae are dense and non-porous with the majority of the pore volume being contributed by macropores and possibly sub-micropores not revealed by N_2 gas desorption. Slow pyrolyzed rice hulls, on the other hand, showed increased surface area and pore volume/area. Interestingly, the BET surface area for slow pyrolyzed rice hulls was about twice as larger than the flash pyrolyzed char ($\sim$50 m^2/g). For all chars, the largest contribution to pore volume was in the low macropore range >50 nm. Yet, for pore area, large contributions from the mesopores was apparent. These results indicated a significant presence of both macro- and mesopores. These results corroborate the qualitative surface roughness analysis of the previous section where slow-pyrolyzed chars shows higher and lower macroporosity for rice hulls and microalgae, respectively.

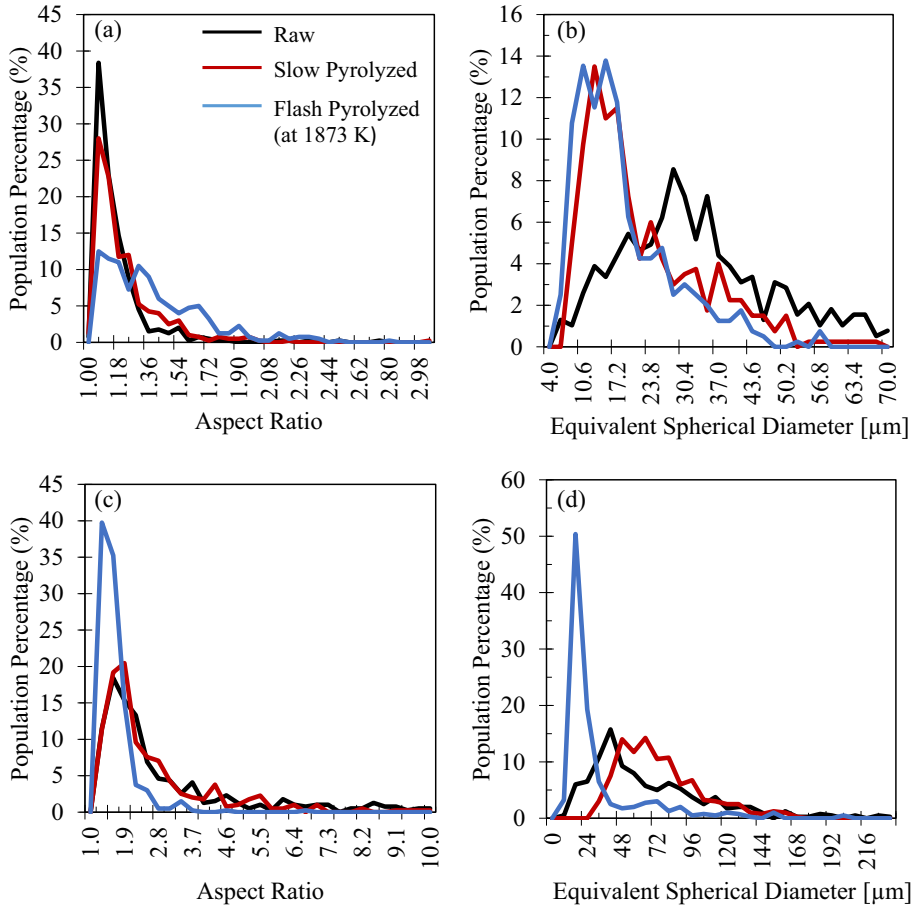

Fig. 4. Aspect ratios and equivalent spherical diameters for (a)-(b) microalgae, (c)-(d) rice hulls, and their chars derived under slow and flash heating conditions.

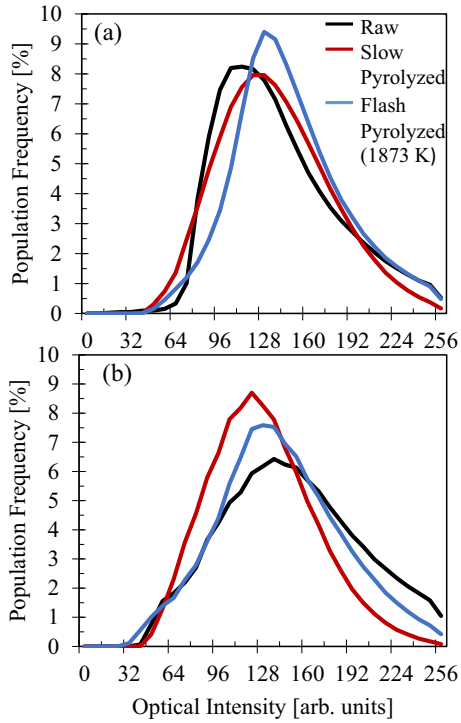

Fig. 5. Pixel density analysis for microalgae, rice hulls, and their chars derived under slow and flash heating conditions.

3.1.4. Apparent reactivity

Gasification reactivity is the apparent gasification rate based on mass loss upon reaction with an oxidant, usually O_2, H_2O, or CO_2. This study chose CO_2 reactivity at 1273 K in a thermogravimeter to correlate physical and morphological properties with apparent reactivity. The universal gas-solid reaction rate constant increases with increasing temperature according to Arrhenius kinetics. At some point while temperature is increasing, the reaction rate becomes faster than the rate of diffusion of reactants into the boundary layer and/or pores of the solid. Likewise, product gases can be prevented from diffusing out of the particle, inhibiting the overall reaction rate. CO_2 gasification follows a Langmuir-Hinshelwood type mechanism for monolayer formation, surface dissociation, and subsequent reaction and desorption. In high temperature gasification processes, the intrinsic reaction rate will be obscured by other physical phenomena such as diffusion and may reveal information about the underlying pore structure of the char.

Fig. 6 displays the reactivity of (a) microalgae char and (b) rice hull char with respect to conversion. In absolute terms, microalgae char was much less reactive than rice hull char and likely due to the differences in initial surface area, porosity, and for flash pyrolyzed chars, the formation of graphitic structures. Slow pyrolyzed char reactivity was also generally higher than flash pyrolyzed in the conversion range 20–90%. This result was interesting because slow pyrolyzed microalgae char was shown to have low surface area and pore volume.

For microalgae, at lower flash heating rates, the char seems to have been activated for enhanced reactivity initially, denoted by high surface area and pore volume. However, at the higher flash heating rates this enhanced reactivity is non-existent and the

Table 3
BET surface areas and BJH pore volumes for microalgae, rice hulls, and their respective carbonaceous residues generated in slow and flash heating conditions (performed in triplicate).

	Microalgae Char					Rice Hull Char				
dry wt%	5 K/min	1573 K	1673 K	1773 K	1873 K	5 K/min	1573 K	1673 K	1773 K	1873 K
C	71.8	85.2	86.2	87.0	78.8	49.4	45.7	43.7	42.7	38.1
H	1.06	1.16	1.22	0.77	0.85	1.55	1.04	0.57	0.73	0.68
O (diff)	7.69	2.08	2.26	1.64	1.42	1.23	0.36	0.25	0.31	0.54
N	4.31	1.16	0.76	0.36	0	3.97	1.90	1.05	0.68	0
S	0.02	0.57	0.66	1.28	1.92	0.02	0.11	0.10	0.10	0.38
Ash	15.1	9.86	8.90	8.97	17.2	43.8	50.9	54.3	55.5	61.1
C_1 molar basis, dry and ash free										
O/C	0.045	0.010	0.007	0.003	0.000	0.060	0.031	0.018	0.012	0.000
H/C	0.176	0.162	0.169	0.105	0.128	0.374	0.271	0.155	0.204	0.213
N/C	0.092	0.021	0.022	0.016	0.015	0.021	0.007	0.005	0.006	0.012
S/C	0.000	0.003	0.003	0.006	0.009	0.000	0.001	0.001	0.001	0.004

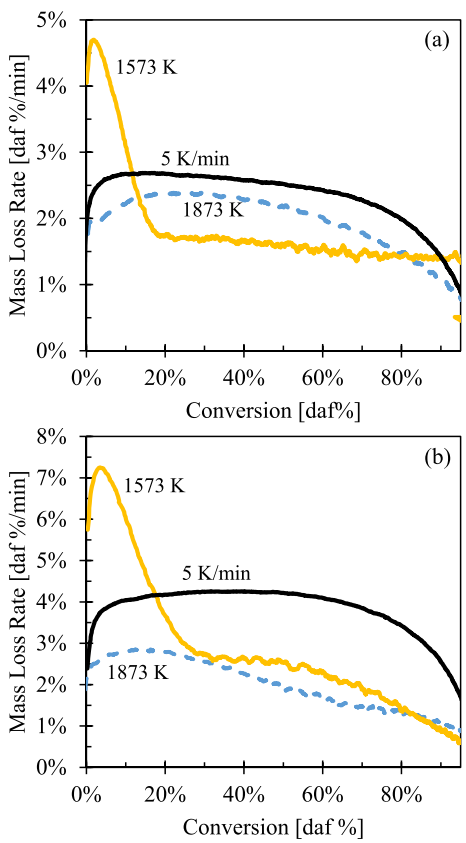

Fig. 6. Apparent reactivity curves for chars from (a) microalgae and (b) rice hulls derived under slow and flash heating conditions.

shape of the reactivity curves is altered. At 1773 K, there may be molecular rearrangement of carbon atoms to form graphitic carbon, forming a new pore structure that reacts differently at higher conversions. This initial elevated activation of reactivity is also probably eliminated by secondary reaction processes, including gasification of the highly reactive portions of the char, thereby revealing the true pore structure of the char.

Rice hulls exhibited similar behavior in that flash pyrolyzed chars up to 1873 K demonstrated increased initial reactivity then a dramatically reduced reactivity that was only slightly higher than the general reactivity of microalgae for conversions greater than 20%. However, at 1873 K, the high initial reactivity is eliminated, again likely due to reaction with volatiles within the system during pyrolysis.

3.2. Gas product yields

The gaseous fraction represented the majority of products formed, approximately 60% and 75% by weight of flash pyrolyzed microalgae and rice hulls, respectively (total unaccounted mass of 5–7%). Because of the high fraction of syngas products, the overall process can be compared to gasification technologies despite the pyrolytic basis. In fact, solely because of the high temperatures of the gas phase combined with moderate residence times, the syngas constituents were found to be primarily hydrogen and carbon monoxide gases for the temperature range studied (Table 4). These results were commensurate with predictions from thermodynamic equilibrium calculations using the software FactSage. The measured values of gas-phase constituents were obtained at steady-state operation with a maximum variability of 10% from the reported value.

The results also indicate increasing hydrogen and carbon monoxide yields with increasing temperature. It is likely that water was also present within the syngas mixture, especially as the gases cooled allowing the water-gas shift reaction to proceed. For both biomass feed materials, the results trended toward reaching the calculated equilibrium values. Since equilibrium predicts primarily H_2, CO, and $C_{(s)}$ at temperature above ~873 K with little change in gas composition up to and past the maximum temperature tested in this study, the system can be said to have a strong kinetic driving force, which is an extremely uncommon operating regime for both biomass pyrolysis and gasification reactors.

3.3. Flash pyrolysis process synthesis

3.3.1. Characteristic time analysis

The flash pyrolysis of carbonaceous materials is a heat-transfer limited process. In the configuration studied, radiative heat trans-

Table 4
Gas-phase product distribution from the flash pyrolysis of microalgae and rice hulls in the temperature range of 1573–1873 K as compared to thermodynamic equilibrium calculated values.

Sample	BET surface area [m^2/g]	BJH pore volume [cm^3/g]
Microalgae		
Virgin	0.56 ± 0.13	0.008 ± 0.003
5 K/min	0.56 ± 0.07	0.002 ± 0.001
1573 K	31.3 ± 0.2	0.171 ± 0.006
1873 K	49.4 ± 0.3	0.135 ± 0.010
Rice Hulls		
Virgin	4.21 ± 0.06	0.009 ± 0.002
5 K/min	89.4 ± 0.5	0.385 ± 0.015
1573 K	24.0 ± 0.4	0.148 ± 0.012
1873 K	68.8 ± 0.3	0.375 ± 0.023

fer from the tube wall to the surface of the particle is the primary mode of particle heating, leading to internal conduction of this surface radiation to heat the particle throughout. It was previously shown that a reaction front can adequately model this process of extreme heat transfer limitation, validly assuming the pyrolytic reactions proceed as a reaction front through the particle (Palumbo and Weimer, 2015). However, it was also noted that particle size was the largest factor affecting the time to complete the pyrolysis process.

Fig. 7 displays the characteristic time regimes for pyrolysis numbers with reference to radiation to the surface of a particle ($Py_R = t_{pyrolysis}/t_{radiation}$), internal conduction ($Py_R = t_{pyrolysis}/t_{conduction}$), and the convective flow of reaction products out of the particle ($Py_R = t_{pyrolysis}/t_{convection}$). Pyrolysis numbers are dimensionless orders-of-magnitude measures for comparing competing chemical and physical phenomena with respect to an 'intrinsic' pyrolysis reaction rate. Since the pyrolysis of biomass does not have a single intrinsic rate, an apparent pyrolysis rate was taken from Chan et al. (1985). The remaining values required to calculate characteristic times are the same as those reported in Palumbo and Weimer (2015). Two particle sizes were chosen that correspond to approximated equivalent spherical diameters of microalgae and rice hulls.

The results of the characteristic time analysis show that the process is, indeed, heat-transfer limited, and particularly by radiative heat transfer (Py_R) to the surface of the particle for the particle sizes studied. Internal conduction (Py_C) is also limiting to the overall process, but closer to a transitional regime. The convective mass transfer of pyrolysis products (Py_M) was shown to be relatively slow compared to the overall pyrolysis reaction. This would allow secondary pyrolysis reactions to occur within the particle as the particle continues to heat up and propagate a reaction front to its center. These secondary reactions may include gasification reactions where oxidizing gases react with the char matrix, creating more macropores and causing attrition of the particle into highly reactive fines that agglomerate with the larger char particles upon downstream deposition. Nevertheless, these results indicate that a high temperature pyrolysis process can only be hastened with smaller particle sizes or with increased radiative flux to the surface of the particles.

3.3.2. Solarthermal processing

Direct and indirect solarthermal reactor systems have been contemplated and demonstrated (Maag and Steinfeld, 2010; Martinek and Weimer, 2013), especially for fixing carbon from thermochemical processing of biomass (Agrawal and Singh, 2010; Mallapragada, 2013). Both configurations are characterized by high radiative flux to the reacting medium, usually aided by an opaque absorber that is preferably a reactant, such as a biomass particle. Using solarthermal inputs to drive a thermochemical conversion process represents a high standard of sustainable production practices for fuels, chemicals, and carbon capture. High temperature flash pyrolysis fits within the domain of operating capability for these types of systems (Zeng, 2017). A conceptual framework of how this may be implemented in shown in Fig. 8, neglecting many of the downstream unit operations that are possible given a wide array of end-uses for each of the product fractions.

In Table 5, high-level design parameters are used to calculate operational outputs for a high temperature solarthermal pyrolysis process using experimental results of gas and char yields from the drop-tube experiments detailed above. Design details such as cavity type, tower height, materials of construction, secondary concentration, and heliostat field layout are ignored but considered implicit within the calculation. An approach similar to that shown in Palumbo et al. (2015) and Kaniyal et al. (2013) was used, primarily with Eqs. (1) and (2), where solar absorption efficiency of the receiver, η_{abs}, is calculated as a function of the temperature of the cavity or absorber, T_g, concentration ratio, $\widetilde{C}$, and a nominal direct normal solar incidence, I, of 1 kW/m^2. The concentration ratio is largely affected by the secondary concentrator in order to minimize re-radiation losses, but a range of 2000–4000 was chosen to correspond to practical systems. Similarly, a fixed total process design power, or reactor heat duty, $\dot{Q}_{sol,net}$, was used to calculate the total heliostat area required, A_{field}, product flow rates and calorific value of the product syngas assuming a heliostat solar collection efficiency, η_{field}, of 70%. Conductive heat losses, $\dot{Q}_{loss}$, were assumed at 30% and 50% of the total design power at 1573 K and 1873 K, respectively.

$$\eta_{abs} = 1 - \left(\frac{\sigma T_g^4}{I\,C}\right) \tag{1}$$

$$\dot{Q}_{sol,net} = \eta_{abs}\eta_{field}A_{field}I - \dot{Q}_{loss} \tag{2}$$

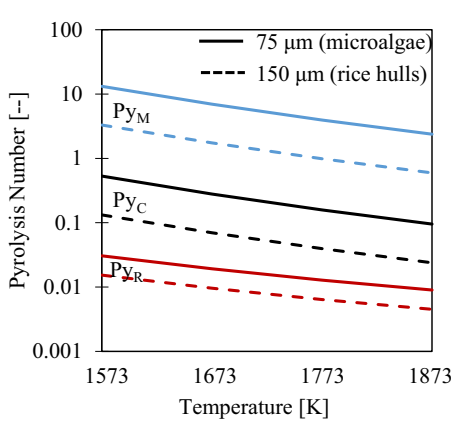

Fig. 7. Pyrolysis numbers for the temperature range of flash heating conditions studied and averaged equivalent spherical diameters for microalgae (75 µm) and rice hulls (150 µm).

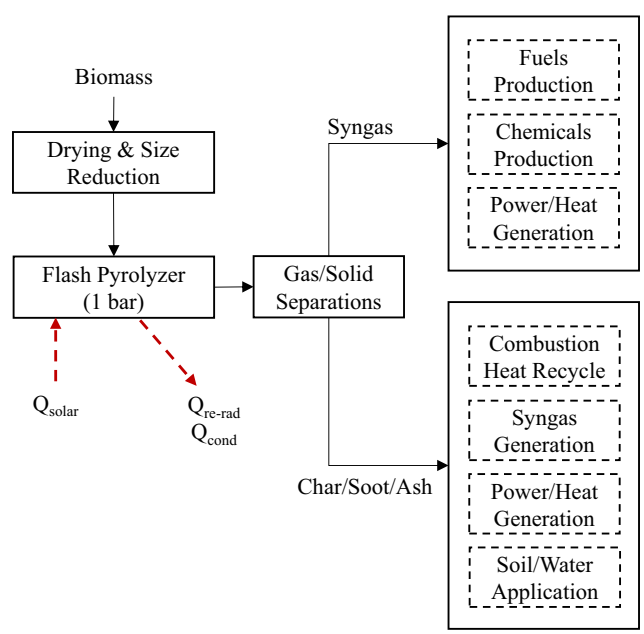

Fig. 8. Block flow diagram depicting the processing options of products derived from high temperature flash pyrolysis of biomass using solarthermal energy.

Table 5
A conceptual solarthermal framework for high temperature flash pyrolysis of biomass including calculated heliostat area, biomass flow rate, and product flow rates for four cases.

Design parameter	Case I	Case II	Case III	Case IV
Reactor temperature [K]	1573	1573	1873	1873
Biomass selection	Microalgae	Rice Hulls	Microalgae	Rice Hulls
Design power (reactor heat duty) [MW]	100			
Average daily solar incidence [kW h/m^2/day]	6			
Direct normalized solar radiation intensity [kW/m^2]	1			
Insolation time [h/day]	10			
Solar field collection efficiency	70%			
Concentration ratio	2000	2000	4000	4000
Receiver conductive and convective heat losses [MW]	$0.3 \cdot Q_{sol,net}$	$0.3 \cdot Q_{sol,net}$	$0.5 \cdot Q_{sol,net}$	$0.5 \cdot Q_{sol,net}$
Dry biomass flow rate [t/h]	150	150	100	100
Calculated performance metrics				
Minimum heliostat area [m^2]	224,700	224,700	259,600	259,600
Gas production [Nm^3/h]	1,47,500	1,80,780	1,47,200	1,44,900
Syngas calorific value [kW]	243	297	237	234
Solids production [kg/h]	107	73.5	58.0	48.0

The overall enthalpy of reaction calculated from equilibrium suggests a slightly exothermic reaction process, indicating that the total biomass flow rate would be governed by the heat transfer-limiting processes within the reacting medium as opposed to the delivered power from the sun. Therefore, a fixed biomass flow rate was used for each temperature based on practical throughputs for a 100 MW system. However, the results in Table 5 are illustrative of a solarthermal process and would necessarily have heat and mass transfer limitations that would need to be determined experimentally in order to evaluate the true maximum loading of biomass for a given tube diameter and length.

Since rice hulls contained a larger fraction of oxygen than microalgae, the productivity of carbonaceous solids was significantly more for the latter process at both temperature cases. Conversely, the calorific value of syngas derived from rice hull processing was much greater than that of microalgae for the same temperatures. While the basic characteristics of the composition and quality of products derived from high temperature flash pyrolysis were common for both biomass feed materials, the process performances were shown to be dramatically different. A desired end-use of thermochemical conversion products, then, must be connected to the specific biomass used and operating conditions used for obtaining useful products such that one can avoid producing undesired products altogether.

4. Conclusions

Presented was an unconventional thermochemical processing technique that cradles the classifications of flash pyrolysis and gasification, using the biomass' own high oxygen content as the oxidizing agent, thereby forming syngas and a carbonaceous residue as the primary products. Microalgae and rice hulls were studied given their substantial difference in biomolecular and atomic compositions. Process performance in the temperature range of 1573–1873 K were characterized by solid and gas yields and compositions. The solid product was further characterized in terms of composition, morphology, and reactivity as preliminary indicators for further processing, though no specific end-use was targeted. Overall, the extreme conditions of the system resulted in solid residues that were similar between the two biomass starting materials with small differences in absolute reactivity. Likewise, the gas composition tended toward achieving equilibrium for each biomass. Perhaps the largest difference that requires further study was the behavior of the inorganic fractions of the starting materials, leading to the formation of crystalline silica structures in rice hull char and graphitic structures in microalgae char. Briefly addressed was the implementation of a solarthermal pyrolysis process with calculated performance metrics using experimental results. A solarthermal system could yield high calorific value syngas and a substantial volume of solid residue for a number of downstream applications. Therefore, the system represents a versatile and simple processing method for converting biomass into useable intermediate compounds to address sustainable production of fuels, chemicals, power, soil amendments, and water treatment materials.

Declaration of interests

The authors declared that there is no conflict of interest.

Acknowledgements

The authors wish to thank the following organizations for their financial support: U.S. Department of Education GAANN Renewable and Sustainable Energy Fellowship, National Science Foundation REU Program, University of Colorado at Boulder UROP, and the Colorado Center for Biorefining and Biofuels.

Appendix A. Supplementary material

Supplementary data to this article can be found online at https://doi.org/10.1016/j.ces.2018.11.029.

References

Aarum, I. et al., 2017. The effect of flash pyrolysis temperature on compositional variability of pyrolyzates from birch lignin. J. Anal. Appl. Pyrol. 127, 211–222.
Agrawal, R., Sikdar, S.K., 2012. Energy, environment and sustainability challenges and opportunities for chemical engineers. Curr. Opin. Chem. Eng. 1 (3), 201–203.
Agrawal, R., Singh, N.R., 2010. Solar energy to biofuels, in annual review of chemical and biomolecular engineering. In: Prausnitz, J.M., Doherty, M.F., Segalman, R.A. (Eds.), Annual Reviews: Palo Alto, pp. 343–364.
Arregi, A. et al., 2018. Evaluation of thermochemical routes for hydrogen production from biomass: a review. Energy Convers. Manage. 165, 696–719.
Asadullah, M. et al., 2010. Effects of biomass char structure on its gasification reactivity. Bioresour. Technol. 101 (20), 7935–7943.
Babu, B.V., 2008. Biomass pyrolysis: a state-of-the-art review. Biofuels Bioproducts Biorefining-Biofpr 2 (5), 393–414.
Bahng, M.K. et al., 2009. Current technologies for analysis of biomass thermochemical processing: a review. Anal. Chim. Acta 651 (2), 117–138.
Biagini, E., Narducci, P., Tognotti, L., 2008. Size and structural characterization of lignin-cellulosic fuels after the rapid devolatilization. Fuel 87 (2), 177–186.
Brewer, C.E. et al., 2009. Characterization of biochar from fast pyrolysis and gasification systems. Environ. Prog. Sustain. Energy 28 (3), 386–396.
Brown, R.C., Stevens, C., 2011. Thermochemical Processing of Biomass: Conversion into Fuels, Chemicals and Power. Wiley.
Cao, X.Y. et al., 2012. Characterization of wood chars produced at different temperatures using advanced solid-state C-13 NMR spectroscopic techniques. Energy Fuels 26 (9), 5983–5991.

Cetin, E. et al., 2004. Influence of pyrolysis conditions on the structure and gasification reactivity of biomass chars. Fuel 83 (16), 2139–2150.
Cetin, E., Gupta, R., Moghtaderi, B., 2005. Effect of pyrolysis pressure and heating rate on radiata pine char structure and apparent gasification reactivity. Fuel 84 (10), 1328–1334.
Cha, J.S. et al., 2016. Production and utilization of biochar: a review. J. Ind. Eng. Chem. 40, 1–15.
Chan, W.C.R., Kelbon, M., Krieger, B.B., 1985. Modeling and experimental-verification of physical and chemical processes during pyrolysis of a large biomass particle. Fuel 64 (11), 1505–1513.
Devi, L., Ptasinski, K.J., Janssen, F., 2003. A review of the primary measures for tar elimination in biomass gasification processes. Biomass Bioenergy 24 (2), 125–140.
Di Blasi, C., 2008. Modeling chemical and physical processes of wood and biomass pyrolysis. Prog. Energy Combust. Sci. 34 (1), 47–90.
Di Blasi, C., Hernandez, E.G., Santoro, A., 2000. Radiative pyrolysis of single moist wood particles. Ind. Eng. Chem. Res. 39 (4), 873–882.
Dufour, A. et al., 2011. Modelling intra-particle phenomena of biomass pyrolysis. Chem. Eng. Res. Des. 89 (10A), 2136–2146.
Dufour, A. et al., 2011. Evolution of aromatic tar composition in relation to methane and ethylene from biomass pyrolysis-gasification. Energy Fuels 25 (9), 4182–4189.
Dupont, C. et al., 2009. Biomass pyrolysis: kinetic modelling and experimental validation under high temperature and flash heating rate conditions. J. Anal. Appl. Pyrol. 85 (1–2), 260–267.
Garcia-Nunez, J.A. et al., 2017. Historical developments of pyrolysis reactors: a review. Energy Fuels 31 (6), 5751–5775.
Janse, A.M.C., Westerhout, R.W.J., Prins, W., 2000. Modelling of flash pyrolysis of a single wood particle. Chem. Eng. Process. 39 (3), 239–252.
Kaniyal, A.A., van Eyk, P.J., Nathan, G.J., 2013. Dynamic modeling of the coproduction of liquid fuels and electricity from a hybrid solar gasifier with various fuel blends. Energy Fuels 27 (6), 3556–3569.
Lede, J., 2010. Biomass pyrolysis: comments on some sources of confusions in the definitions of temperatures and heating rates. Energies 3 (4), 886–898.
Lee, J.W. et al., 2010. Characterization of biochars produced from cornstovers for soil amendment. Environ. Sci. Technol. 44 (20), 7970–7974.
Maag, G., Steinfeld, A., 2010. Design of a 10 MW particle-flow reactor for syngas production by steam-gasification of carbonaceous feedstock using concentrated solar energy. Energy Fuels 24, 6540–6547.
Maliutina, K. et al., 2017. Comparative study on flash pyrolysis characteristics of microalgal and lignocellulosic biomass in entrained-flow reactor. Energy Convers. Manage. 151, 426–438.
Mallapragada, D.S. et al., 2013. Sun-to-fuel assessment of routes for fixing CO2 as liquid fuel. Ind. Eng. Chem. Res. 52 (14), 5136–5144.
Manya, J.J., 2012. Pyrolysis for biochar purposes: a review to establish current knowledge gaps and research needs. Environ. Sci. Technol. 46 (15), 7939–7954.
Martinek, J., Weimer, A.W., 2013. Design considerations for a multiple tube solar reactor. Sol. Energy 90, 68–83.
Milne, T.A.E., Evans, R.J., Abatzoglou, N., 1998. Biomass Gasifier "Tars": Their Nature, Formation, and Conversion. NREL, Golden, CO, p. 204.
Palumbo, A.W., Sorli, J.C., Weimer, A.W., 2015. High temperature thermochemical processing of biomass and methane for high conversion and selectivity to H2-enriched syngas. Appl. Energy 157, 13–24.
Palumbo, A.W., Weimer, A.W., 2015. Heat transfer-limited flash pyrolysis of woody biomass: overall reaction rate and time analysis using an integral model with experimental support. J. Anal. Appl. Pyrol. 113, 474–482.
Qin, K. et al., 2012. Biomass gasification behavior in an entrained flow reactor: gas product distribution and soot formation. Energy Fuels 26 (9), 5992–6002.
Qin, K. et al., 2013. Characterization of residual particulates from biomass entrained flow gasification. Energy Fuels 27 (1), 262–270.
Qureshi, K.M. et al., 2018. A technical review on semi-continuous and continuous pyrolysis process of biomass to bio-oil. J. Anal. Appl. Pyrol. 131, 52–75.
Scott, D.S., Piskorz, J., 1982. The flash pyrolysis of aspen-poplar wood. Can. J. Chem. Eng. 60 (5), 666–674.
Singh, N.R. et al., 2010. Estimation of liquid fuel yields from biomass. Environ. Sci. Technol. 44 (13), 5298–5305.
Sun, H. et al., 2012. Multiple controls on the chemical and physical structure of biochars. Ind. Eng. Chem. Res. 51 (9), 3587–3597.
Tanger, Paul et al., 2013. Biomass for thermochemical conversion: targets and challenges. Front. Plant Sci. 4, 1–20.
Vamvuka, D., 2011. Bio-oil, solid and gaseous biofuels from biomass pyrolysis processes – an overview. Int. J. Energy Res. 35 (10), 835–862.
Woodruff, R.B., Kreider, P., Weimer, A.W., 2012. A novel brush feeder for the pneumatic delivery of dispersed small particles at steady feed rates. Powder Technol. 229, 45–50.
Zeng, K. et al., 2017. Solar pyrolysis of carbonaceous feedstocks: a review. Sol. Energy 156, 73–92.